



Cite this: *Med. Chem. Commun.*, 2014, 5, 1172

Design of glycosyltransferase inhibitors targeting human O-GlcNAc transferase (OGT)[†]

Shuai Wang,^a David L. Shen,^{bc} Dominique Lafont,^a Anne-Sophie Vercoutter-Edouart,^d Marlène Mortuaire,^d Yun Shi,^c Ofelia Maniti,^a Agnès Girard-Egrot,^a Tony Lefebvre,^d B. Mario Pinto,^c David Vocadlo^{bc} and Sébastien Vidal^{*a}

Inhibition of glycosyltransferases requires the design of neutral inhibitors to allow cell permeation in contrast to their natural dianionic substrates. O-GlcNAc transferase (OGT) is a key enzyme involved in dynamic glycosylation of cytosolic and nuclear proteins in competition with phosphorylation. Designing OGT inhibitors is of prime interest for the better understanding of its biological implications. Introduction of a pyridine moiety as a pyrophosphate surrogate was evaluated, which provided moderate *in vitro* inhibition of OGT. Docking studies highlighted some key features for the binding of the designed inhibitors to the catalytic site of OGT where the carbohydrate moiety did not occupy its natural position but rather turned away and pointed to the solvent outside the catalytic pocket. Further investigation with cellular assays did not provide inhibition of OGT. This lack of OGT inhibition was rationalized with a permeation assay which revealed the sequestration of the inhibitors at the membrane.

Received 17th February 2014
Accepted 20th March 2014

DOI: 10.1039/c4md00063c

www.rsc.org/medchemcomm

Introduction

O-GlcNAcylation (O-linked β-N-acetylglucosamylation) is an abundant post-translational modification found predominantly on cytosolic and nuclear proteins.¹ O-GlcNAcylation is conserved among all metazoans studied to date,^{2–8} and it has been proposed to regulate fundamental cellular processes including cell signaling,⁹ cell cycle,^{10,11} and circadian clock function.¹²

In contrast to the more structurally complex glycosylation occurring within the secretory pathway, O-GlcNAcylation is dynamic in that it can be installed and removed from proteins several times during the lifetime of the polypeptide backbone.^{13,14} Transfer of the N-acetylglucosamine (GlcNAc) residue from the nucleotide-sugar UDP-GlcNAc onto target proteins is catalyzed by the glycosyltransferase known as O-GlcNAc transferase (OGT, uridine diphospho-N-acetylglucosamine:polypeptide

β-N-acetylglucosaminyltransferase or O-GlcNAc transferase).^{15–18} The glycoside hydrolase O-GlcNAcase (OGA, *exo*-β-N-acetylglucosaminidase) catalyzes removal of the GlcNAc moiety from proteins.¹⁹ OGT (EC. 2.4.1.255) is assigned to the GT41 family of the glycosyltransferase superfamily within the CAZY (Carbohydrate-Active enZYme) classification system.²⁰ GT41 family members adopt a GTB fold, which comprises two Rossmann-like domains separated by a cleft. These GT41 enzymes are inverting glycosyltransferases, meaning that the overall glycosyl transfer reaction proceeds with inversion of stereochemistry at the anomeric center. OGT possesses a series of tetratricopeptide repeats (TPRs), which are generally involved in protein–protein interactions.²¹ In mammals, three OGT isoforms have been described and they differ primarily in the number of their TPRs.¹⁸ Nuclear and cytoplasmic OGT (ncOGT), the best-characterized and the longest isoform, contains 13.5 TPRs, sOGT only contains 2.5 TPRs and mOGT, which is generated by alternative splicing, contains 8.5 TPRs and a MTS (Mitochondrial Targeting Sequence).

The regulation of OGT and the mechanism by which it recognizes modification sites remains an open question, though the recently solved structure of a large fragment of OGT is greatly facilitating progress in this area.²² The emerging roles of OGT in fundamental cellular processes as well as diseases including for example cancer and neurodegeneration make tools that can perturb the OGT function of considerable interest. The generation of potent and selective inhibitors of OGT is consequently a topic of current interest. Relatively few compounds, however, have been identified that can inhibit this

^aInstitut de Chimie et Biochimie Moléculaires et Supramoléculaires, CO2-Glyco and GEMBAS, UMR 5246, CNRS, Université Claude Bernard Lyon 1, Université de Lyon, 43 Boulevard du 11 Novembre 1918, F-69222 Villeurbanne, France. E-mail: sebastien.vidal@univ-lyon1.fr; Fax: +33 472 448 109; Tel: +33 472 448 349

^bDepartment of Chemistry, Simon Fraser University, Burnaby, British Columbia, Canada V5A 1S6

^cDepartment of Molecular Biology and Biochemistry, Simon Fraser University, Burnaby, British Columbia, Canada V5A 1S6

^dUnité de Glycobiologie Structurale et Fonctionnelle, UMR CNRS/USTL no 8576, IFR 147, Université des Sciences et Technologies de Lille, Avenue Mendeleiev, 59655 Villeneuve d'Ascq, France

[†] Electronic supplementary information (ESI) available: Experimental procedures for the synthesis of compounds 2–14 and NMR spectra, cellular OGT inhibition assays, and permeation assays. See DOI: 10.1039/c4md00063c

enzyme^{23,24} making the design of OGT inhibitors a continuing challenge.

The rational design of GT inhibitors generally involves the synthesis of acceptor, bi-substrate, and donor analogues. Donor analogues of UDP-GlcNAc can bind tightly, but the dianionic pyrophosphate bridge limits the permeability of such compounds for use in cells. Several donor analogues have been assessed as inhibitors including UDP-C-GlcNAc, UDP-S-GlcNAc, and UDP-5S-GlcNAc (Fig. 1). These compounds, however, cannot permeate into cells making the design of donor analogues, in which the pyrophosphate bridge is replaced, of considerable interest. Alloxan is a cell permeable inhibitor of OGT but suffers from promiscuous inhibition of multiple targets, which leads to cellular toxicity. A benzoxazolinone derivative was identified using high-throughput screening²⁴ and was later shown to be an irreversible OGT inhibitor.²⁵

The present work focuses on the design of OGT inhibitors following a glycomimetic approach^{26–28} as analogues of the natural UDP-GlcNAc substrate. The syntheses will use common azido-functionalized precursors and conjugations will be achieved through either azide-alkyne cycloaddition or Staudinger-Villarrasa amide bond formation (Fig. 2). The amide or triazole functionalities were chosen as potential hydrogen bond donors or acceptors in view of additional and beneficial interactions with the enzyme's active site. The resulting *N*-glycosidic linkages were also selected due to their analogy with natural *N*-linked oligosaccharides and also better stability *in vivo* as recently reported for *N*-glycosyl triazoles.^{29,30}

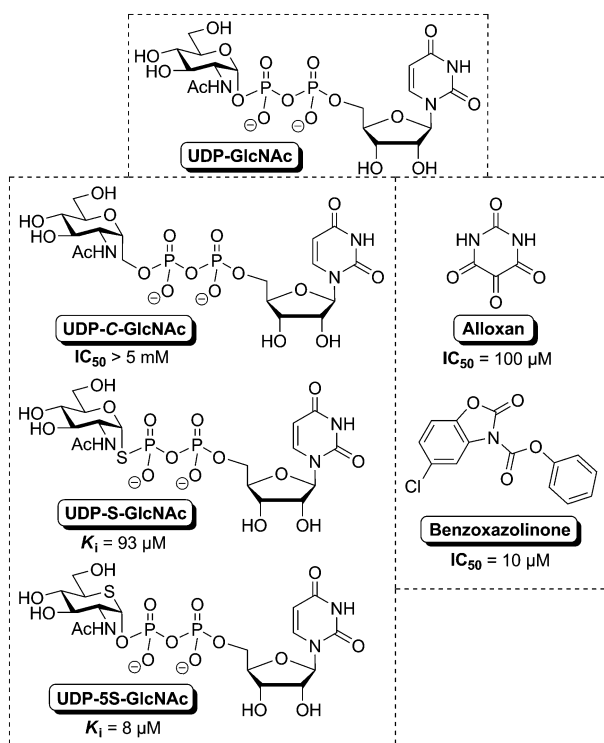


Fig. 1 Structures of UDP-GlcNAc and (left) known non-neutral inhibitors of OGT based on UDP-GlcNAc analogues and (right) neutral OGT inhibitors identified to date.

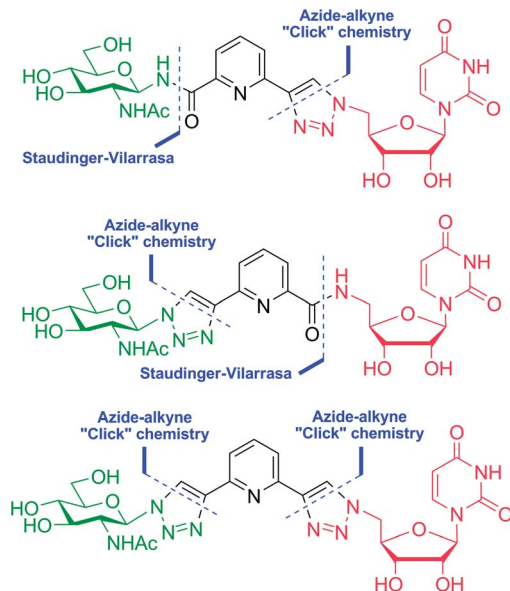
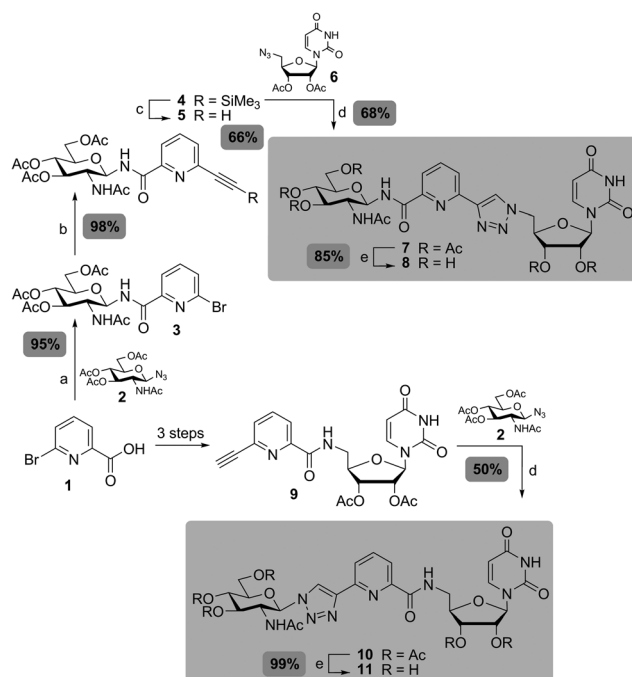


Fig. 2 Structures of three UDP-GlcNAc analogues and an overview of the retrosynthetic strategies to access these compounds.

Results and discussion

Synthesis of UDP-GlcNAc analogues

Starting from 6-bromopicolinic acid **1**, two pathways using the same synthesis procedures afforded the UDP-GlcNAc analogues **8** and **11** with variations at the positions of the

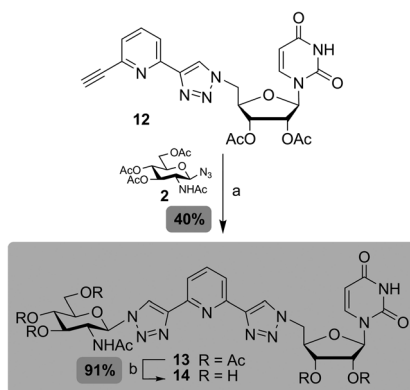


Scheme 1 Synthesis of two triazole/amide containing UDP-GlcNAc analogues **8** and **11**. Reagents and conditions: (a) PMe_3 , DIC, HOBT, and THF. (b) $Me_3SiC\equiv CH$, $Pd(PPh_3)_4$, CuI, iPr_2NH , and PhMe. (c) nBu_4NF and MeOH. (d) $CuSO_4$, sodium ascorbate, and $tBuOH-H_2O$ and (e) NaOMe and MeOH.

amide and triazole conjugations (Scheme 1). The Staudinger-Vilarrasa conjugation^{31–33} of 6-bromo-picolinic acid **1** with glycosyl azide **2** afforded the desired *N*-acylated glycopyranosyl amine **3** in 95% yield. Sonogashira coupling of this aryl bromide with trimethylsilylacetylene afforded intermediate **4**. Purification of the silyl-protected intermediate **4** was troublesome and this held for the other Sonogashira reactions performed in this series. As a result, cleavage of the silyl groups was carried out directly to provide alkyne derivative **5**. This two-step process was used in all cases, providing the desired alkynes in good yields. CuAAC conjugation with 2',3'-di-*O*-acetyl-5'-azido-5'-deoxy-uridine **6**³⁴ afforded the acetylated derivative **7**, which was converted to the UDP-GlcNAc analogue **8** under Zemplén conditions. Similarly, 6-bromopicolinic acid **1** was converted to alkyne **9**,³⁵ which was used in the CuAAC coupling with glycosyl azide **2** to provide the acetylated precursor **10**. Final deacetylation gave the second UDP-GlcNAc analogue **11**.

The UDP-GlcNAc analogues incorporating two triazole moieties were prepared from alkyne **12** (Scheme 2).³⁵ CuAAC conjugation³⁶ with glycosyl azide **2** led to acetylated precursor **13**, which was converted under Zemplén conditions to the third UDP-GlcNAc analogue **14**.

Using these approaches, three UDP-GlcNAc analogues **8**, **11**, and **14** were synthesized using a minimum number of synthesis steps in good overall yields (Fig. 3). A series of UDP-Glc analogues **15–17** were also prepared³⁵ using the same synthesis procedures (Fig. 3). These compounds incorporated the same amide and triazole moieties. The rationale for preparing these was to use them as negative controls in the inhibition assays. Two UDP analogues **18** and **19** were also synthesized and selected as potential OGT inhibitors since UDP is a known inhibitor of glycosyltransferases including OGT. Finally, the UDP-Gal analogue **20** (Fig. 3) was synthesized in a parallel study on galactosyltransferase inhibition.³⁵ This analogue was used as a positive control in the permeation assays in comparison to the inhibitors tested in the present study.



Scheme 2 Synthesis of a bis-triazole containing UDP-GlcNAc analogue **14**. Reagents and conditions: (a) CuI, *i*Pr₂NEt, and DMF and (b) NaOMe and MeOH.

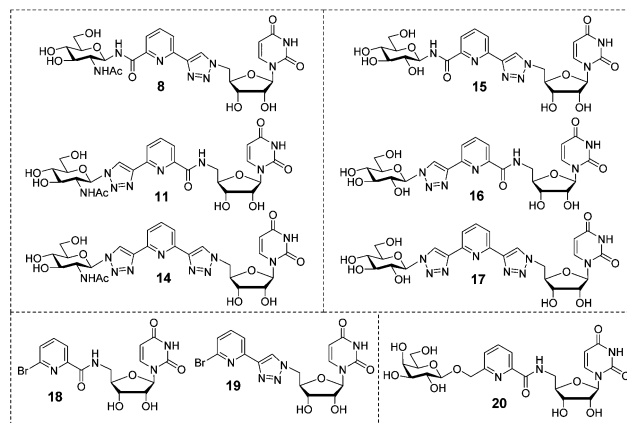


Fig. 3 Structures of the six analogues (**8**, **11**, **14**, **15**, **16** and **17**) and two UDP analogues (**18** and **19**) evaluated as OGT inhibitors and of a UDP-Gal analogue (**20**) used as a positive control in permeation assays.

Enzymatic studies (IC₅₀ and K_i measurements) with human OGT *in vitro*

These eight synthesized NDP-sugar analogues were evaluated as inhibitors of human OGT *in vitro* (Table 1). These compounds were first assayed at 50 μM concentration and the inhibition was measured at this concentration. This 50 μM concentration was selected as a first pass since it facilitates the detection of genuine inhibitors rather than compounds having indirect effects on the OGT activity. This initial assay revealed that most compounds showed little inhibition at 50 μM. Nevertheless, three analogues (**15**, **17** and **19**) showed greater than 10% inhibition of hOGT suggesting that these could be legitimate OGT inhibitors and therefore these compounds were selected for further study. Surprisingly, the most promising compounds are the UDP-Glc analogues **15** and **17** while the UDP-GlcNAc analogues **8**, **11** and **14** were quite poor inhibitors. The third compound of interest is the UDP analogue **19**. Measurement of the K_i value for the best inhibitor (**15**) by Dixon analysis was carried out (see ESI†), providing a value of 422 μM, which though moderate in potency represents a reasonable level of inhibition for such a derivative. The Dixon analysis performed, however, does not allow us to distinguish whether the inhibitor is competitive or not.

Table 1 Enzymatic inhibition of hOGT

Analyte	Inhibitor	% Inhibition at 50 μM	IC ₅₀ (μM)	K _i (μM)
UDP-GlcNAc	8	3.0 ± 0.2	n.d.	n.d.
	11	9.7 ± 0.7	n.d.	n.d.
	14	6.7 ± 0.4	n.d.	n.d.
UDP-Glc	15	18 ± 1	340 ± 20	420 ± 10
	16	4.2 ± 0.2	n.d.	n.d.
	17	13.3 ± 0.9	1600 ± 300	n.d.
UDP	18	7.6 ± 0.1	n.d.	n.d.
	19	15.5 ± 0.9	710 ± 20	n.d.

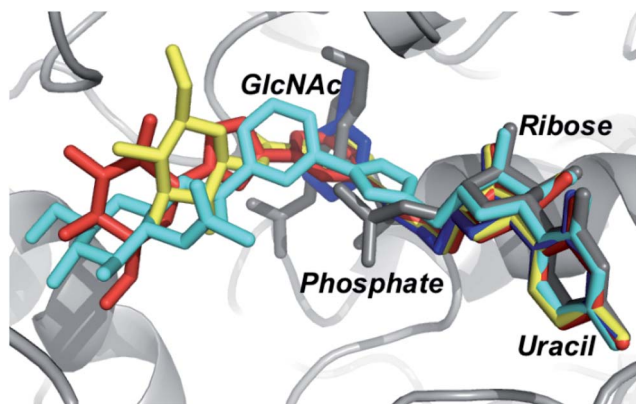


Fig. 4 Overview of the best docking poses in comparison with the natural substrate UDP-GlcNAc (grey: OGT, grey sticks: UDP-GlcNAc; cyan sticks: **8**; yellow sticks: **15**; red sticks: **17**; blue sticks: **19**). Different regions of UDP-GlcNAc are labeled in black.

Modeling inhibitors within the active site of OGT

To gain insight into the binding of these compounds to OGT, docking of several of these inhibitors including **8**, **15**, **17**, and **19** was carried out using the known structure of OGT in complex with UDP-GlcNAc (PDB 4GZ5) as the template. The best ranking pose was selected from the docking of each OGT inhibitor (Fig. 4). The uridine portion of all four inhibitors showed near

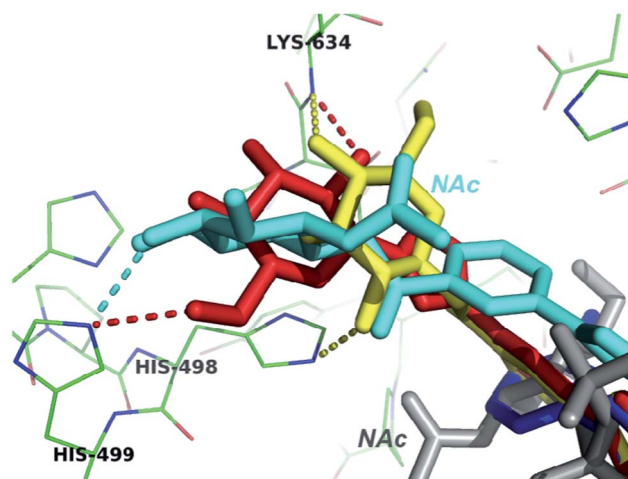


Fig. 6 Inhibitor binding within the Glc/GlcNAc portion (grey sticks: UDP-GlcNAc; cyan sticks: **8**; yellow sticks: **15**; red sticks: **17**; blue sticks: **19**; all other lines represent OGT residues). Dashed lines indicate possible hydrogen bonds from different inhibitors. The acetamido group of UDP-GlcNAc and **8** is also labeled in grey and cyan, respectively.

perfect overlap, with almost identical binding modes to that of UDP-GlcNAc. This also agrees with X-ray structures showing relatively static binding modes of the uridine portion in different ligands.³⁷

The triazole linkers in **15**, **17**, and **19** share the same orientation and location, with N2 accepting one hydrogen bond from the hydroxyl group of Thr922 and N3 accepting another from the amide backbone of Thr921 (Fig. 5). These polar interactions from the triazole resemble those from the β -phosphate of UDP-GlcNAc, and the absence of such hydrogen bonds in **8** could contribute to its weak inhibitory activity.

However, the binding mode of the natural substrate was not mimicked with respect to the GlcNAc residue (Fig. 6). The bromopyridine moiety in **19** partially overlapped with the GlcNAc ring of UDP-GlcNAc, with its ring nitrogen accepting a hydrogen bond from the Thr921 hydroxyl group. Yet, an orientation perpendicular to that of GlcNAc was adopted by the pyridine ring of **15** and **17**; **8** did not contact this space at all. In the glucose-GlcNAc end of the molecules, both **15** and **17** could form hydrogen bonds with His498, His499, and Lys634, whereas **8** could be involved in a hydrogen bonding interaction with His499 (Fig. 6). Of note, the acetamido group of **8** showed no direct interaction with the enzyme, and its presence may also have forced this molecule to adopt a different and less energetically favorable conformation compared to its glucose counterpart **15**.

In summary, compound **19** exhibited the best substrate mimicry in terms of binding geometry, while the other three inhibitors extended too far past the sugar-binding pocket and placed the pyranose moiety in a completely different region of the enzyme active site. These modeling studies therefore reveal why the change of the sugar residue from that of the natural substrate GlcNAc to Glc does not have a significant effect on binding even though OGT has an established preference for GlcNAc over Glc.²²

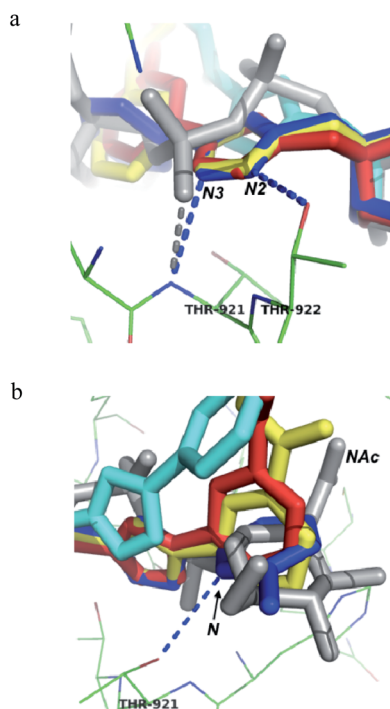


Fig. 5 Detailed comparison of substrate and inhibitor binding (grey sticks: UDP-GlcNAc; cyan sticks: **8**; yellow sticks: **15**; red sticks: **17**; blue sticks: **19**; all other lines represent OGT residues). (a) Hydrogen bonds (blue dashed lines) were formed with N2 and N3 of the triazole; the polar interaction between the β -phosphate of UDP-GlcNAc and Thr921 is also shown (grey dashed line) for comparison. (b) The pyridine nitrogen of **19** accepted a hydrogen bond.

Cellular OGT inhibition and permeation assays

Given that derivative **15** shows some inhibition of OGT, the next logical step was to evaluate these derivatives under cell culture conditions to see whether they could block the OGT action in a biological setting. Compounds **8**, **11**, and **14–18** were also selected since the permeability of these compounds into cells and their cellular efficacy are difficult to estimate solely on the basis of *in vitro* inhibition data. The inhibition of *O*-GlcNAcylation in a cell based assay was not observed for any of the designed inhibitors (see ESI†). This lack of inhibition at the cell level could be the result of either (1) poor permeation of the inhibitors through the cell membrane or (2) decomposition or elimination of the inhibitors by the cell machinery. To clarify the question of permeation of these inhibitors, additional studies were performed. We have designed an assay in which the cell membrane is mimicked by a lipid bilayer of liposomes. The penetration of organic molecules into the liposomes was detected through their intrinsic UV properties. Two candidates were tested here: UDP-Gal analogue **20**, synthesized in a parallel study on galactosyltransferases³⁵ and used in this work as a model compound for permeation assays, and UDP-Glc analogue **15** designed herein (see ESI†). The permeation of the molecules could not be detected and the conclusion of this evaluation is that these compounds are either adsorbed at the surface of the liposome or could not cross the lipidic bilayer.

Conclusions

The synthesis of NDP-sugar analogues incorporating a pyridine moiety as a replacement for the pyrophosphate moiety was achieved through a combination of Staudinger–Vilarrasa and azide–alkyne cycloaddition. The compounds obtained were then evaluated as substrate-based inhibitors of OGT mimicking UDP-GlcNAc. *In vitro* assays on human OGT provided only poor to moderate inhibition with the best compound displaying an inhibition constant (K_i) value of 420 μM . Docking studies were then performed to better rationalize the inhibition pattern observed for these inhibitors. The inhibition studies do not enable the inhibitors to be assigned as competitive, however, the modelling studies support binding at the active site. Specifically, the uracil moiety of these molecules was always found to bind in an almost identical manner as seen for the natural UDP-GlcNAc substrate and is likely responsible for most of the binding to the enzyme. The pyrophosphate group of the natural substrate forms H-bonds with the enzyme's active site and the triazole moieties of these analogues could reproduce such interactions. Nevertheless, a major change was observed for the position of the carbohydrate moiety (either GlcNAc or Glc) which pointed out into the solvent and therefore was positioned outside the binding pocket. This observation explains why the glucose-based analogue was also an inhibitor like the expected GlcNAc analogue. This observation was very similar to our previous report of galactosyltransferases in which the carbohydrate moiety was also located outside of the enzyme's catalytic site based on crystallographic studies of enzyme–inhibitor complexes.³⁵ Cellular assays were then performed to

evaluate the potential applications of such inhibitors but no activity could be observed on different cell lines even at high concentrations (up to 500 μM). A permeation assay designed using liposomes showed that these inhibitors do not permeate through the liposome membrane, allowing us to conclude that the lack of inhibition observed in cellular assays was probably due to the poor permeability of the compounds through the cell membrane. The level of moderate inhibition observed, coupled with the docking studies, suggests that the linkers identified in this study serve as a replacement for the pyrophosphate unit but that they fail to position the sugar residue in the appropriate position. Furthermore, these compounds lack the needed permeability, suggesting that further changes are needed to improve both the orientation of the sugar mimicking element as well as to enhance the permeability. Further refinement in the rationale design of glycosyltransferase inhibitors is still necessary to obtain cell permeable inhibitors with potential applications in cell assays or even *in vivo*.

Experimental section

General methods

All reagents were obtained from commercial sources and used without further purification. Dichloromethane was distilled over CaH_2 . Methanol was distilled over Mg/I_2 . All reactions were performed under an argon atmosphere unless otherwise stated. Thin-layer chromatography (TLC) was carried out on aluminum sheets coated with silica gel 60 F₂₅₄ (Merck). TLC plates were inspected using UV light ($\lambda = 254 \text{ nm}$) and developed by treatment with a mixture of 10% H_2SO_4 in $\text{EtOH-H}_2\text{O}$ (1 : 1 v/v) followed by heating. Silica gel column chromatography was performed with silica gel Si 60 (40–63 μm). NMR spectra were recorded at 293 K, unless otherwise stated, using Bruker 300, 400 or 500 MHz spectrometers. Chemical shifts are referenced relative to deuterated solvent residual peaks. The following abbreviations are used to explain the observed multiplicities: s, singlet; d, doublet; t, triplet; q, quadruplet; m, multiplet and bs, broad singlet. Complete signal assignments were based on 1D and 2D NMR (COSY, HSQC and HMBC correlations). High resolution (HR-ESI-QToF) mass spectra were recorded using a Bruker MicroToF-Q II XL spectrometer. Optical rotations were measured using a Perkin Elmer polarimeter and values are given in $10^{-1} \text{ deg cm}^2 \text{ g}^{-1}$.

General protocol for Staudinger–Vilarrasa conjugation

The acid (0.466 mmol, 1 eq.) and HOBt (0.839 mmol, 1.8 eq.) were co-evaporated with toluene ($3 \times 5 \text{ mL}$) and THF ($3 \times 5 \text{ mL}$). The mixture was dried under vacuum for 1 h. The mixture was dissolved in dry THF (4 mL) under argon and cooled to 0 °C. DIC (0.839 mmol, 1.8 eq.) was added dropwise at 0 °C. After addition, the ice-bath was removed and the reaction was stirred at r.t. for 30 min. Meanwhile, the azide (0.699 mmol, 1.5 eq.) was dissolved in dry THF (4 mL) under argon and cooled to 0 °C. PMe_3 (0.932 mmol, 2 eq.) was added and the reaction was stirred at 0 °C. After 30 min, the solution was transferred into a flask containing the acid–HOBt solution at 0 °C. The flask was

washed with THF (4 mL) and the solution was transferred. The resulting reaction mixture was stirred at 0 °C for 1 h, then allowed to reach r.t. and stirred for an additional 16 h. The reaction mixture was diluted with water (60 mL) and extracted with EtOAc (4 × 60 mL). The combined organic layers were washed with sat. Na₂CO₃ (60 mL), H₂O (60 mL) and brine (60 mL), dried (Na₂SO₄) and concentrated. The residue was purified by silica gel column chromatography (PE to EtOAc) to afford the desired amide.

General protocol for Sharpless CuAAC conjugation

To a solution of the alkyne (0.19 mmol, 1 eq.) and the azide (0.19 mmol, 1 eq.) in *t*BuOH–H₂O (1/1, 5.6 mL/280 μL) were added CuSO₄ (0.11 mmol, 0.6 eq.) and sodium ascorbate (0.228 mmol, 1.2 eq.). The reaction was stirred at 35 °C for 24 h then diluted with water (20 mL) and extracted with CH₂Cl₂ (3 × 30 mL). The combined organic layers were dried (Na₂SO₄) and concentrated. The residue was purified by silica gel column chromatography to afford the desired triazole.

General protocol for Meldal CuAAC conjugation

*i*Pr₂NEt (0.036 mmol, 0.25 eq.) was added into a flask containing the azide (0.14 mmol, 1 eq.), the alkyne (0.14 mmol, 1 eq.) and CuI (0.01 mmol, 0.1 eq.) in DMF (2 mL). The reaction was stirred at r.t. overnight. After 24 h, the solution was diluted with EtOAc (50 mL), washed with sat. Na₂CO₃ (2 × 25 mL) and H₂O (30 mL). The combined aqueous layers were extracted with EtOAc (3 × 30 mL). The combined organic layers were dried (Na₂SO₄) and concentrated. The residue was purified by silica gel column chromatography to afford the desired triazole.

General protocol for Sonogashira reaction

Bromo-arene (1.0 mmol, 1 eq.), Pd(PPh₃)₄ (0.1 mmol, 0.1 eq.) and CuI (0.1 mmol, 0.1 eq.) were dissolved in toluene (25 mL) and the solution was degassed with argon. Then, trimethylsilylacetylene (3.0 mmol, 3 eq.) and diisopropylamine (2.2 mmol, 2.2 eq.) were added. The reaction was stirred for 48 h at r.t. protected from light then poured into sat. NH₄Cl (100 mL). The aqueous layer was extracted with CH₂Cl₂ (3 × 100 mL). The combined organic layers were washed with H₂O (100 mL) and brine (100 mL), dried (Na₂SO₄) and concentrated. The residue was then purified by silica gel column chromatography to afford the desired product.

Radioactive OGT inhibition assays

The ability of small molecules to inhibit the OGT activity was assessed using radiolabelled [³H]-UDP-GlcNAc (American Radiolabel) as the donor and recombinant nup62 as the acceptor.³⁸ Assays contained 10 μM nup62 and 1 μM UDP-GlcNAc for the assay (constant specific activity of 0.8 Ci mmol⁻¹ of [³H]-UDP-GlcNAc) or 50 μM UDP-GlcNAc (constant specific activity of 0.35 Ci mmol⁻¹ of [³H]-UDP-GlcNAc), 100 nM hOGT, and various concentrations of the inhibitor (for *K*_i values a range of concentrations including 1000, 500, 250, 125, 62.5 and 31.25 μM were used and for IC₅₀ values a range from 3000 to 100

μM was used). The reaction was initiated by the addition of the enzyme with a pipette and incubated at 37 °C for 1 h (a time for which linear rates are obtained under these assay conditions). The reactions were placed on ice after 1 h of incubation and then immediately applied to a 1.5 by 3 cm piece of nitrocellulose membrane (BioRad) and allowed to air dry. The quantity of protein loaded onto each piece of nitrocellulose was at least ten times less than the binding capacity of the membrane (as detailed in the manufacturer's protocol). The membranes were washed with four consecutive large volumes (100 mL) of PBS and air dried. The pieces of membrane were loaded into scintillation vials, 4 mL of scintillation fluid (Amersham) was added, and the levels of tritium were quantified using a liquid scintillation counter (Beckman LS6000). All assays were done in triplicate (2 minutes for sample counting). The *K*_i value is calculated from an equation generated based on the establishment of the Dixon plot of each inhibitor and where it is intersected with the 1/*V*_{max}.

Docking studies

The O-GlcNAc transferase (OGT) crystal structure (PDB: 4GZ5) was protonated by Molprobitry,³⁹ and chain B was extracted after removal of water, ions, and the substrate to serve as the model macromolecule in the docking study. All four OGT inhibitors were built with the ribose and GlcNAc (Glc) ring conformations identical to those of the natural substrate in the crystal structure.³⁷ The macromolecule and four inhibitors were then processed by AutoDockTools to remove non-polar hydrogens.⁴⁰ A grid box centered on the position of the natural substrate was constructed using 24 × 24 × 24 points and a spacing of 1 Å. Subsequently, each inhibitor was docked into OGT by AutoDock Vina,⁴¹ which automatically calculates the grid maps and clusters the results, with the value of the exhaustiveness parameter being 32.

Acknowledgements

The authors thank the Université Claude Bernard Lyon 1 and the CNRS for financial support. S.V. is grateful for financial support from the COST Action CM-1102 MultiGlycoNano. S.W. thanks the Ministère de l'Enseignement Supérieur et de la Recherche for a PhD stipend under the international program. Dr F. Albriex, C. Duchamp and N. Henriques are gratefully acknowledged for mass spectrometry analyses. A.S.V.E. and T.L. thank the CNRS and the Comité du Nord de la Ligue Contre le Cancer for financial supports. D.J.V. and B.M.P. thank the Natural Sciences and Engineering Council of Canada (NSERC) for their support. D.J.V. thanks the Canada Research Chairs (CRC) program for support as the CRC in Chemical Glycobiology and NSERC for the award of an EWR Steacie Memorial Fellowship. Wesley Zandberg and Lehua Deng are thanked for preparing the UDP-5S-GlcNAc.

Notes and references

- 1 G. W. Hart, M. P. Housley and C. Slawson, *Nature*, 2007, **446**, 1017–1022.

- 2 D. Nolte and U. Müller, *Mamm. Genome*, 2002, **13**, 62–64.
- 3 G. D. Holt, C. M. Snow, A. Senior, R. S. Haltiwanger, L. Gerace and G. W. Hart, *J. Cell Biol.*, 1987, **104**, 1157–1164.
- 4 N. E. Olszewski, C. M. West, S. O. Sassi and L. M. Hartweck, *Biochim. Biophys. Acta*, 2010, **1800**, 49–56.
- 5 D. A. R. Sinclair, M. Syrzycka, M. S. Macauley, T. Rastgardani, I. Komljenovic, D. J. Vocadlo, H. W. Brock and B. M. Honda, *Proc. Natl. Acad. Sci. U. S. A.*, 2009, **106**, 13427–13432.
- 6 Y. Perez-Cervera, G. Harichaux, J. Schmidt, F. Debierre-Grockiego, V. Dehennaut, U. Bieker, E. Meurice, T. Lefebvre and R. T. Schwarz, *Amino Acids*, 2011, **40**, 847–856.
- 7 A. Shen, H. D. Kamp, A. Gründling and D. E. Higgins, *Genes Dev.*, 2006, **20**, 3283–3295.
- 8 J. d. J. Pérez, N. D. Udeshi, J. Shabanowitz, S. Ciordia, S. Juarez, C. L. Scott, N. E. Olszewski, D. F. Hunt and J. A. Garcia, *Virology*, 2013, **442**, 122–131.
- 9 Q. Zeidan and G. W. Hart, *J. Cell Sci.*, 2010, **123**, 13–22.
- 10 S. Olivier-Van Stichelen, L. Drougat, V. Dehennaut, I. El Yazidi-Belkoura, C. Guinez, A. M. Mir, J. C. Michalski, A. S. Vercoutter-Edouart and T. Lefebvre, *Oncogenesis*, 2012, **1**, e36.
- 11 L. Drougat, S. Olivier-Van Stichelen, M. Mortuaire, F. Foulquier, A.-S. Lacoste, J.-C. Michalski, T. Lefebvre and A.-S. Vercoutter-Edouart, *Biochim. Biophys. Acta*, 2012, **1820**, 1839–1848.
- 12 M.-D. Li, H.-B. Ruan, M. Hughes, J.-S. Lee, J. Singh, S. Jones, M. Nitabach and X. Yang, *Cell Metab.*, 2013, **17**, 303–310.
- 13 E. P. Roquemore, M. R. Chevrier, R. J. Cotter and G. W. Hart, *Biochemistry*, 1996, **35**, 3578–3586.
- 14 R. S. Haltiwanger and G. A. Phillipsberg, *J. Biol. Chem.*, 1997, **272**, 8752–8758.
- 15 R. S. Haltiwanger, G. D. Holt and G. W. Hart, *J. Biol. Chem.*, 1990, **265**, 2563–2568.
- 16 B. D. Lazarus, D. C. Love and J. A. Hanover, *Glycobiology*, 2006, **16**, 415–421.
- 17 R. Hurtado-Guerrero, H. C. Dorfmüller and D. M. F. van Aalten, *Curr. Opin. Struct. Biol.*, 2008, **18**, 551–557.
- 18 D. J. Vocadlo, *Curr. Opin. Chem. Biol.*, 2012, **16**, 488–497.
- 19 L. Wells, Y. Gao, J. A. Mahoney, K. Vosseller, C. Chen, A. Rosen and G. W. Hart, *J. Biol. Chem.*, 2002, **277**, 1755–1761.
- 20 B. L. Cantarel, P. M. Coutinho, C. Rancurel, T. Bernard, V. Lombard and B. Henrissat, *Nucleic Acids Res.*, 2009, **37**, D233–D238.
- 21 M. Jinek, J. Rehwinkel, B. D. Lazarus, E. Izaurralde, J. A. Hanover and E. Conti, *Nat. Struct. Mol. Biol.*, 2004, **11**, 1001–1007.
- 22 M. B. Lazarus, Y. Nam, J. Jiang, P. Sliz and S. Walker, *Nature*, 2011, **469**, 564–567.
- 23 T. M. Gloster, W. F. Zandberg, J. E. Heinonen, D. L. Shen, L. Deng and D. J. Vocadlo, *Nat. Chem. Biol.*, 2011, **7**, 174–181.
- 24 B. J. Gross, B. C. Kraybill and S. Walker, *J. Am. Chem. Soc.*, 2005, **127**, 14588–14589.
- 25 J. Jiang, M. B. Lazarus, L. Pasquina, P. Sliz and S. Walker, *Nat. Chem. Biol.*, 2012, **8**, 72–77.
- 26 P. Sears and C.-H. Wong, *Angew. Chem., Int. Ed.*, 1999, **38**, 2300–2324.
- 27 D. C. Koester, A. Holkenbrink and D. B. Werz, *Synthesis*, 2010, **2010**, 3217–3242.
- 28 B. Ernst and J. L. Magnani, *Nat. Rev. Drug Discovery*, 2009, **8**, 661–677.
- 29 C. J. Carroux, J. Moeker, J. Motte, M. Lopez, L. F. Bornaghi, K. Katneni, E. Ryan, J. Morizzi, D. M. Shackelford, S. A. Charman and S.-A. Poulsen, *Bioorg. Med. Chem. Lett.*, 2013, **23**, 455–459.
- 30 C. J. Carroux, G. M. Rankin, J. Moeker, L. F. Bornaghi, K. Katneni, J. Morizzi, S. A. Charman, D. Vullo, C. T. Supuran and S.-A. Poulsen, *J. Med. Chem.*, 2013, **56**, 9623–9634.
- 31 H. Chapuis and P. Strazewski, *Tetrahedron*, 2006, **62**, 12108–12115.
- 32 J. Burés, M. Martin, F. Urpi and J. Vilarrasa, *J. Org. Chem.*, 2009, **74**, 2203–2206.
- 33 J. Garcia, F. Urpi and J. Vilarrasa, *Tetrahedron Lett.*, 1984, **25**, 4841–4844.
- 34 H. Chen, J. Zhao, Y. Li, F. Shen, X. Li, Q. Yin, Z. Qin, X. Yan, Y. Wang, P. Zhang and J. Zhang, *Bioorg. Med. Chem. Lett.*, 2011, **21**, 574–576.
- 35 S. Wang, J. A. Cuesta-Seijo, D. Lafont, M. M. Palcic and S. Vidal, *Chem.–Eur. J.*, 2013, **19**, 15346–15357.
- 36 M. Meldal and C. W. Tornøe, *Chem. Rev.*, 2008, **108**, 2952–3015.
- 37 M. B. Lazarus, J. Jiang, T. M. Gloster, W. F. Zandberg, G. E. Whitworth, D. J. Vocadlo and S. Walker, *Nat. Chem. Biol.*, 2012, **8**, 966–968.
- 38 D. L. Shen, T. M. Gloster, S. A. Yuzwa and D. J. Vocadlo, *J. Biol. Chem.*, 2012, **287**, 15395–15408.
- 39 V. B. Chen, W. B. Arendall III, J. J. Headd, D. A. Keedy, R. M. Immormino, G. J. Kapral, L. W. Murray, J. S. Richardson and D. C. Richardson, *Acta Crystallogr., Sect. D: Biol. Crystallogr.*, 2010, **66**, 12–21.
- 40 G. M. Morris, R. Huey, W. Lindstrom, M. F. Sanner, R. K. Belew, D. S. Goodsell and A. J. Olson, *J. Comput. Chem.*, 2009, **30**, 2785–2791.
- 41 O. Trott and A. J. Olson, *J. Comput. Chem.*, 2010, **31**, 455–461.